

# The UAVSAR Phased Array Aperture

Neil Chamberlain, Mark Zawadzki, Greg Sadowy, Eric Oakes, Kyle Brown, Richard Hodges,  
Jet Propulsion Laboratory, California Institute of Technology  
4800 Oak Grove Drive, Pasadena, CA 91109

Neil.F.Chamberlain@jpl.nasa.gov, Mark. S.Zawadzki@jpl.nasa.gov, Gregory.A.Sadowy@jpl.nasa.gov,  
Eric.Oakes@jpl.nasa.gov, Kyle.M.Brown@jpl.nasa.gov, Richard.E.Hodges@jpl.nasa.gov

*Abstract*—This paper describes the development of a patch antenna array for an L-band repeat-pass interferometric synthetic aperture radar (InSAR) instrument that is to be flown on an unmanned aerial vehicle (UAV). The antenna operates at a center frequency of 1.2575 GHz and with a bandwidth of 80 MHz, consistent with a number of radar instruments that JPL has previously flown. The antenna is designed to radiate orthogonal linear polarizations in order to facilitate fully-polarimetric measurements. Beam-pointing requirements for repeat-pass SAR interferometry necessitate electronic scanning in azimuth over a range of  $\pm 20$  degrees in order to compensate for aircraft yaw. Beam-steering is accomplished by transmit / receive (T/R) modules and a beamforming network implemented in a stripline circuit board.

This paper, while providing an overview of phased array architecture, focuses on the electromagnetic design of the antenna tiles and associated interconnects. An important aspect of the design of this antenna is that it has an amplitude taper of 10dB in the elevation direction. This is to reduce multipath reflections from the wing that would otherwise be detrimental to interferometric radar measurements. This taper is provided by coupling networks in the interconnect circuits as opposed to attenuating the output of the T/R modules.

Details are given of material choices and fabrication techniques that meet the demanding environmental conditions that the antenna must operate in. Predicted array performance is reported in terms of co-polarized and cross-polarized far-field antenna patterns, and also in terms of active reflection coefficient.<sup>1,2</sup>

## TABLE OF CONTENTS

TABLE OF CONTENTS.....	1
1. INTRODUCTION.....	1
2. PREDICTED PERFORMANCE.....	7
3. CONCLUSIONS.....	11
4. REFERENCES .....	11
5. BIOGRAPHIES .....	11

## 1. INTRODUCTION

UAVSAR (unmanned aerial vehicle synthetic aperture radar) is an airborne, polarimetric, repeat-pass, interferometric radar system operating at L-band. The primary mission of UAVSAR is to accurately map crustal deformations associated with natural hazards, such as volcanoes and earthquakes. Additional science studies include rapidly moving glaciers and volumetric studies in ice and vegetation. Topographic information is derived from phase measurements that, in turn, are obtained from two or more passes over a given area.

The need to make accurate phase measurements imposes constraints on both the radar platform and the instrument itself; particularly on the antenna. These constraints are essentially as follows. First, the radar platform must fly within a 10m diameter tube centered around the path of first flight. This is accomplished by using an inertial guidance / GPS system, coupled with a precision auto-pilot system. Second, the antenna beam must be slewed to compensate for aircraft yaw variations on subsequent passes. This is accomplished using an active phased array that scans in azimuth. Third, the radar signature must be relatively free of systematic phase variations, due primarily to temperature variations in the antenna and beamforming network. This is accomplished through the use of materials with low coefficients of thermal expansion, temperature control and compensation of the antenna transmit / receive (T/R) modules, and design techniques that mitigate against other thermal and mechanical perturbations. In tandem with these high-level requirements, the antenna development for this instrument is subject to other design constraints, which include:

1. An antenna pattern that produces relatively small perturbations in the phase and amplitude of the far-field pattern due to multipath scattering from the aircraft.
2. Design that is impervious to condensation and water vapor in a wide range of operational environments.
3. Design that is amenable to rapid prototyping and development on an aggressive schedule.
4. Design that is amenable to accurate and rapid analysis of antenna performance, both in terms of antenna

1  
2

patterns, antenna impedance, and the interaction of the antenna with the aircraft.

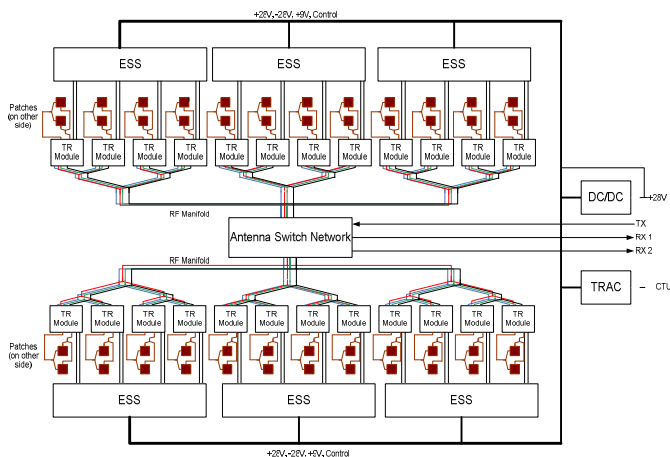
5. Thermal cycling over large temperature range of  $-70^{\circ}\text{C}$  to  $+50^{\circ}\text{C}$
6. Mass and profile consistent with a pod-based accommodation below the radar platform.
7. Design that is amenable to repair of failure in the interconnects, damage due to runway-debris, or failure of a T/R module.

These requirements are in addition to the standard antenna-related requirements of gain, sidelobe, impedance match, and cross-polarization performance, that are discussed later.

The following section gives an overview of the phased array antenna as a system, and subsequent sections describe the (passive aperture) part of this system in more detail.

### Antenna Overview

A block diagram of the phased array antenna is shown in Fig. 1. The aperture comprises 48 patch antenna elements arranged as an array of 4 elements in elevation by 12 elements in azimuth. The elevation spacing of the elements is 10cm and the azimuth spacing is 12.5cm. The corresponding aperture size is 0.4m by 1.5m, but the antenna groundplane is larger than this (0.6m by 1.75m) in order to accommodate the various antenna electronics sub-assemblies, and also to facilitate operation with existing P-band equipment. The aperture is fabricated as an array of 6 antenna tiles, each of which has 4 elements in elevation by 2 elements in azimuth. The antenna tiles are bonded to an aluminum honeycomb panel by means of conductive epoxy. The aluminum honeycomb panel forms the mechanical backbone of the antenna, with radiating elements on one side and antenna electronics on the other side. The antenna tiles are covered by a protective radome, which is fabricated from fiberglass face sheets and a fiberglass honeycomb core.



The microstrip patch elements are single-layer patches measuring approximately 8cm square on a low-permittivity dielectric honeycomb, also fabricated from fiberglass honeycomb. The patch elements are fed with two probes for each polarization in order to provide the required bandwidth over scan. The elements are capable of radiating both horizontal (H) and vertical (V) polarization.

There are 24 T/R modules feeding elements pair-wise in elevation. This architecture facilitates beam scanning in azimuth also enables short-baseline cross-track interferometry between the antenna upper and lower halves, while using the minimum number of T/R modules. A bank of four T/R modules is fed from a single energy storage sub-system – essentially a custom DC\_DC converter that provides 32V DC power at up to 40A pulsed. The T/R modules are configured to transmit either an H pulse or a V pulse, and to receive both an H pulse and V pulse simultaneously. The peak power of the T/R modules is 100W, and the maximum duty cycle is 5%. Thus, the average and peak RF powers radiated by the antenna are 81W and 1.6kW, respectively (assuming interconnect losses of 1.7dB). The T/R modules are cooled by means of an air duct that runs along the length of the antenna. The air-velocity in the duct is controlled to maintain a relatively low thermal gradient across the T/R modules.

The element feed networks are configured so that the center two rows of elements receive approximately 10 times the power of the outer two rows; thus implementing an amplitude taper that controls the sidelobe performance near end-fire. These networks, and the hybrid that is required to produce complementary 0 degree and 180 degree excitation of the patch element, are contained in a printed circuit board stripline network that is integrated into the lower face sheet of the 4x2 antenna tile. The tile has SMA connectors on its lower surface that connect to the T/R modules (via a through hole in the aluminum honeycomb panel) by means of coaxial cables. T/R modules connect to RF manifold boards by means of a block assembly of four GPO-type connectors.

Beamforming is implemented by a combination of phase shifters and attenuators in the T/R modules, and by means of a network of printed circuit manifolds. The T/R module vendor is designing custom MMIC circuits to implement the phase shifter and LNA functions of the T/R module. There are four RF manifolds: one for transmit, two for receive (one for H and one for V), and one for calibration. Separate manifolds are provided for the upper and lower halves of the antenna ray to facilitate short baseline cross-track interferometry. Manifolds consists of two 12-way corporate dividers implemented as stripline transmission lines in multi-layer printed circuit boards that are located between the two rows of T/R modules. The common ports of the 12-ways are connected to a switching network that routes receive, transmit and calibrations signals to and from the RF

electronics as required by the current radar operating mode.

DC power and control cables are routed in conduits along the top edge and bottom edge of the antenna. In previous phased array developments, DC power, control, and RF manifold boards have been incorporated into a single printed circuit board [1]. This approach was not feasible for the UAVSAR antenna owing to the larger number of RF manifolds and also because of space constraints on the non radiating side of the antenna.

### Antenna Requirements

The following requirements apply to the UAVSAR antenna aperture.

Table 1. Antenna Requirements for UAVSAR

Parameter	Requirement
Center Frequency	1.2575 GHz
Bandwidth	80 MHz
Polarization	H and V
Gain Flatness	$\leq \pm 0.5$ dB (90% band)
Phase Linearity	$\leq \pm 10^\circ$ (90% band)
Peak Power	$\geq 100$ W per element pair
Average Power	$\geq 5$ W per element pair
Azimuth Beamwidth	$8^\circ \pm 1^\circ$
Elevation Beamwidth	$33^\circ$ to $40^\circ$
Azimuth Scanning Range	$\geq \pm 20^\circ$
Elevation Scanning Range	No requirement
Azimuth Sidelobe, Tx	$\leq -11$ dB
Azimuth Sidelobe, Rx	$\leq -20$ dB
Elevation Sidelobe, Tx & Rx	$\leq -30$ dB (for $ \theta  > 85^\circ$ )
Opposite-side ambiguity	$\leq -20$ dB ( $-65^\circ$ to $-100^\circ$ )
Pattern Cross-Pol	$\leq -25$ dB in main lobe
Peak Gain	$\geq 18$ dB ( $P_{svs} \geq 95$ dBm)
Return Loss	$\geq 10$ dB (at T/R port)
Radome Loss	$\leq 0.5$ dB
Operating temperature	$-70^\circ\text{C}$ to $+50^\circ\text{C}$
Operating Rel. Humidity	0% to 100%
Operation altitude	Sea-level to 60,000'
Lifetime	$\geq 5$ years and $\geq 635$ hours per year

There is a desire to have the array scan beyond  $\pm 20^\circ$  in azimuth, with possibly degraded performance. Additional key requirements for the full electronically steered active array include:

- Pointing resolution of  $1^\circ$  or less
- Pointing accuracy of  $0.8^\circ$  or less
- End-to-end post calibration phase errors of  $2^\circ$  rms or less
- Total antenna mass (including electronics and all structure) of less than 70kg

The design that is elaborated in subsequent sections is compliant with all these requirements, as determined by analysis.

### Aperture Design

The UAVSAR aperture is constructed as an assembly of 6 antenna tiles that are arranged in a horizontal row. This is illustrated in Fig.2. The choice and configuration of the antenna tile (or sub-array) is key to meeting the performance and development requirements of the UAVSAR instrument. First, the tile dimensions of 44cm in elevation by 25cm in azimuth (16 inch by 10 inch) mean that correspondingly sized circuit boards will fit comfortably on a standard 12 inch by 18 inch PCB core with room for tooling holes and coupons. A larger tile (in azimuth) would restrict the number of available vendors who could process the printed circuit boards, and also would suffer more from bowing due to CTE mismatches. Second, the chosen tile configuration facilitates a relatively smooth transition from breadboard development to flight antenna production. The UAVSAR antenna development is predicated on accurate modeling of the full-size array, as verified by the fabrication and antenna range measurement of a single antenna tile.

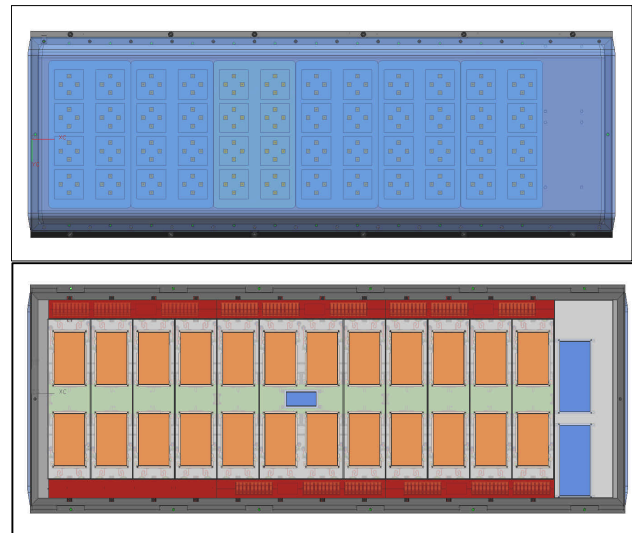


Figure 2. Top: Radiating side (aperture) of UAVSAR phased array. The aperture comprises 6 antenna tiles of 4 elements in elevation and 2 elements in azimuth arranged side-by-side. Bottom: Non-radiating side of antenna array showing T/R modules (orange), power supplies (red), RF manifold boards (green), switching electronics (blue), and antenna groundplane (gray).

Once a 4-by-2 tile has been breadboarded, tested, and validated, it is a relatively simple matter of producing more of these tiles and integrating them into the full-size array. This allows us to produce a full-size flight aperture without having to produce a full-size engineering model, thus reducing cost and development time. Two important features

of the design make this sort of development jump possible; at least for this application. First the antenna tile is full-size in the elevation direction. Thus, once the tile design is proved, one will have a relatively good estimate of antenna performance in the elevation direction, which is critical to meeting the multipath requirement. Second, the design is amenable to moment method-based analysis, meaning that large fractions of the overall aperture can be analyzed to assess performance in the azimuth and elevation directions. Assuming that the tile performance accords with model predictions, then production of the full aperture can proceed with relatively high confidence.

The UAVSAR aperture is shown in cross section in Fig. 3. This figure illustrates the 3 major sub-assemblies of the aperture (from top to bottom)

1. A dielectric honeycomb-based radome of approximately 1.5cm thickness
2. A dielectric honeycomb-based tile of approximately 1.5cm thickness, separated from the radome by 1.5cm
3. An aluminum honeycomb-based groundplane of approximately 2cm thickness

The planar nature of the design makes it amenable to moment method-based analysis, and also allows the radome design to be done concurrently with the tile design. The antenna aperture, as measured from the top of the aluminum honeycomb groundplane to the top of the radome is approximately 4.5cm or 1.8 inch. The entire phase array antenna, as measured from the top of the radome (as oriented in Fig 3.) to the bottom of the largest electronics box on the bottom side (and not including the air duct) measures approximately 12cm or 4.6 inch.

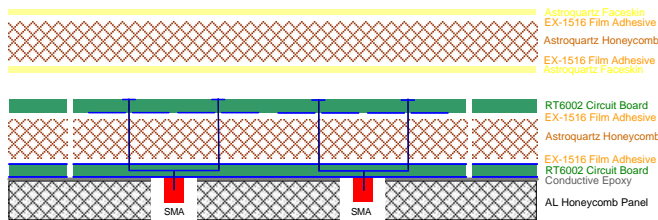


Figure 3. Cross-section through antenna aperture showing radome (yellow face sheets), tile (green face sheets) and aluminum groundplane (black face sheets)

### Tile Design

The UAVSAR antenna tile is illustrated in Fig. 4. An antenna tile comprises an Astroquartz honeycomb sandwiched between two printed circuit board face sheets. The Astroquartz honeycomb has extremely low CTE and is impervious to moisture. The weave of the fibers in the honeycomb facilitates venting of moisture. The printed circuit boards are fabricated from RT/duroid 6002. This

substrate has a very low coefficient of thermal expansion, low RF losses, and relatively low Young's modulus. This yields a circuit board that is temperature stable, able to withstand large numbers temperature cycles without via cracking, and relatively compliant with thermally induced flexures of the underlying aluminum honeycomb groundplane. Tile mass, including conductive epoxy, is 1kg. This represents less than 10% of the total antenna mass (for six tiles).

The top most circuit board contains the patch elements (on the underside) and matching capacitors (on the top side). The matching capacitors tune out the inductance of the probe interconnect. These features are etched on the top of the tile so that they can be trimmed for tuning the breadboard antenna. The bottom most circuit board contains hybrids and power dividers that effect the amplitude tapering and phasing of the signals that drive the patch elements. The  $0^\circ/180^\circ$  phasing is implemented by means of ring hybrids that have been deformed to fit in the available space and interconnect topology. Isolation resistors are mounted on the top side of the bottom circuit board (essentially inside the quartz honeycomb) and SMA connectors are mounted on the bottom side of the interconnect circuit board. It is these connectors that connect to the T/R modules through coaxial cables. The 10dB amplitude tapering is implemented by means of edge-coupled striplines. These circuits have an edge separation of about 2.5 mil, so it is important that the circuit board manufacturer be able to hold close tolerances on these features, and provide a uniform fill of the gap. We chose a fusion bonding process for this and other reasons.

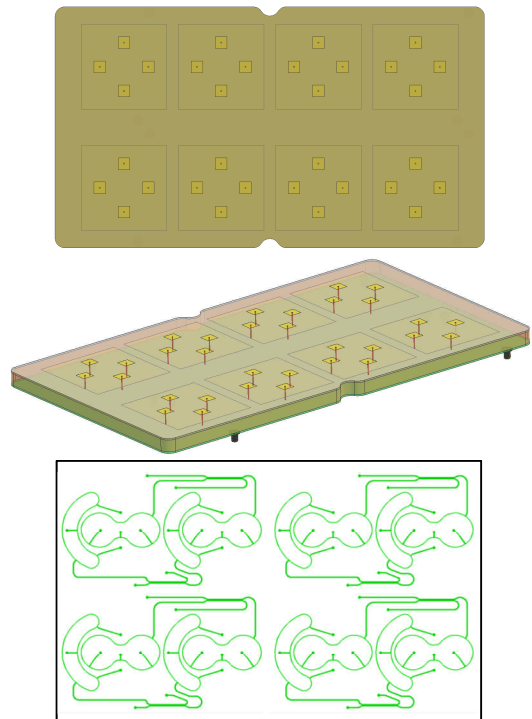


Figure 4. Tile construction. Top: Tile patch layer. Middle: Projected view showing patch layer. Bottom: Tile interconnect layer.

The SMA connectors and probes are installed in vias (through holes) that are counterbored to within a few mil of the stripline. We chose 30 mil cores for the board design (resulting in a 60 mil groundplane to groundplane clearance), which was mainly driven by the design of the 10dB coupler. The upper (patch-layer) circuit board is fabricated on a 60mil core in order to provide a symmetrical stack up. Of course, the full copper ground planes on the lower board prevent this stack up from being perfectly symmetrical, so to minimize CTE mismatches due to these copper ground planes, the tile interconnect board was scored along its mid-point (vertically in Fig. 4) and via-d on either side of the score in order to provide electrical continuity across the score. This helps to reduce bowing in the tile, which after all bonding and curing operations were complete, measured less than 20 mil (0.5mm) at the short edges of the tile. The counterbores on the bottom side of the interconnect board are backfilled with sheet adhesive that is cured in the same cycle as the rest of the tile.

### Element Design

The antenna element is designed as a dual probe-fed single layer microstrip patch. A number of patch interconnects were considered for this application, including single probe-fed designs, aperture-coupled designs, and proximity-coupled designs. JPL has tended to favor probe-fed designs for microstrip array applications due to the mechanical robustness of the design and the fidelity of the electromagnetic modeling. Additionally, balanced feeds tend to have superior scanning performance as the higher order modes are naturally suppressed by the symmetrical feeding arrangement. A dual-probe interconnect was chosen for UAVSAR as a result of this performance advantage and as a consequence of our design heritage.

The patch – groundplane separation (approximately 1.5cm) and the underlying substrate permittivity (approximately 1.1) result in an unscanned 15 dB return loss bandwidth of better than 150MHz, as estimated from an infinite array simulation. The element is capable of scanning to 25 degrees in azimuth for H-pol, and 30 degrees in azimuth for V-pol with an 80 MHz bandwidth and 15dB return loss or better. Larger scan angles are possible at the cost of degraded return loss, which ultimately manifests as a loss of gain.

### Interconnect Design

The tile interconnect network provides connectivity between the T/R modules and patch antenna elements, ensuring that the proper amplitude and phase is fed to each of the antenna ports. The network is essentially a 10dB coupler feeding a 0°/180° hybrid – for each pair of elements in the tile and for each polarization – meaning there are four such circuits in the interconnect board. These are illustrated in Fig. 5.

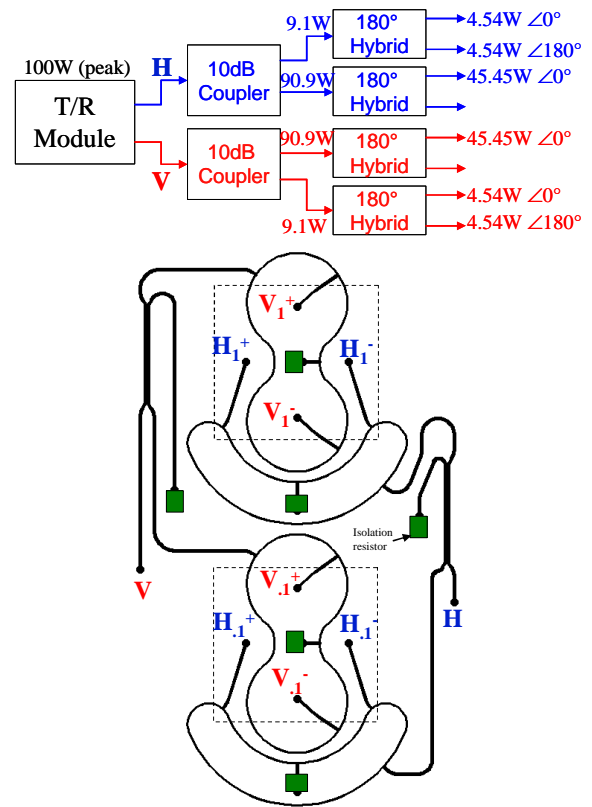


Figure 5. Interconnect network for element pair (lower pair in tile). Top: Block diagram of network. Bottom: Stripline layout showing edge couplers and ring hybrids. There are four such networks in each antenna tile.

The networks for the upper two elements in the tile are rotated 180° in order to connect with the upper row of T/R modules, which are likewise rotated 180° with respect to the lower row.

The striplines are fabricated in 60 mil Rogers RT6002 using a fusion bond process. Fusion bond lamination provides a very clean lamination of RF substrates and eliminates the need to include prepregs or other bonding materials that might otherwise affect the impedance of the lines. The downside of fusion bonding (compared to other techniques) is that fewer vendors tend to have this capability and the quality of the bond is sensitive to temperature, pressure, and the moisture content of the cores.

The interconnect board is ‘connectorized’ in the following way. SMA connectors are attached to the bottom of the board. A 50 mil diameter center pin is soldered to a counterbored via, which in turn connects to the Stripline. Similarly, 50 mil diameter probes protrude from the top of the interconnect board and are likewise soldered to vias that connect to the distribution striplines. The counterbores on the bottom layer are backfilled in order to prevent conductive epoxy (which bonds the tile to the aluminum groundplane) from seeping into the hole and shorting the probe pins. See Fig.6.

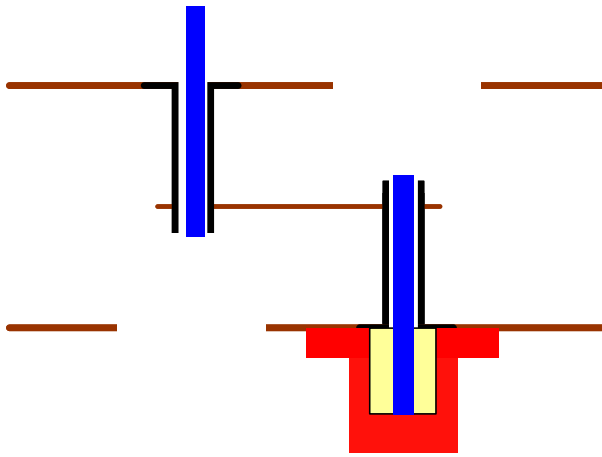


Figure 6. Connector and probe interconnect showing counterbored vias.

Isolation resistors are soldered to the top of the interconnect board and are bonded to a pad using a wire strap. These resistors are large enough to handle 100W CW. In the event that full-power CW testing of the tile is required. The Astroquartz honeycomb must be recessed slightly to accommodate these resistors.

#### *Radome Design.*

The design of the radome is driven by structural and electromagnetic requirements. The radome is essentially a flat quartz honeycomb panel with Astroquartz face sheets. This provides a very strong and electromagnetically transparent covering for the antenna. The thickness of the radome, approximately 1.5cm, is chosen to keep deflections due to wind loading at less than 0.5cm. The radome – tile separation of 1.5cm is chosen to keep phase variations due to such deflections in the radome at an acceptable level.

The face sheets are fabricated in a dry lay-up from prepreg quartz cloth, and the entire radome assembly is cured in a single operation lasting approximately 4 hours. The outer surface of the cured radome is painted with approximately 2 mil of radome paint. Additionally, the radome is tapered along the long side of the antenna so that it blends with the pod wall. This is illustrated in the end view of the antenna shown in Fig. 7.

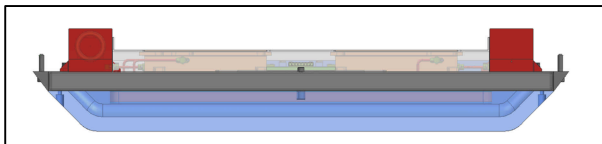


Figure 7. End view of antenna showing radome (light blue). The sides of the radome are tapered to blend with the pod. The ends of the radome are flush with the pod wall to prevent turbulence.

#### *Mechanical and Thermal Design.*

The goal of the antenna mechanical design to provide a stable, temperature-controlled platform for the aperture and active electronics. The structure of the antenna is a 0.75 inch (1.9 cm) thick aluminum honeycomb panel chosen for its stiffness and light weight. By using conductive adhesive to join the antenna tiles to the structure, the face sheet of the structural panel serves as a common continuous groundplane for the aperture. The antenna tile construction and attachment as well as the structural materials of the antenna and radome have been tested extensively to ensure the robustness of the design to the thermal stresses, the maneuver loads, and the vibrational loads of an airborne environment.

The UAVSAR antenna is intended to be compatible with various aircraft platforms and operate over a broad flight envelope. The instrument is able to collect science data at altitudes between 2 and 18 km, at airspeeds from 100 to 250 m/s, at ambient air temperatures of -70 to +50 deg C, and at 0 to 100% relative humidity. The thermal design of the antenna must keep the electronics, particularly the T/R modules, within their operating temperature limits and maintain the temperature gradient across the modules below 10 deg C over this flight envelope. The active electronics are convectively cooled by ducting ambient air through a nozzle in the nose cone of the unpressurized pod across the active side of the antenna. Obviously, the properties of this ducted air vary significantly with altitude, airspeed, and location on Earth. Thermal modeling and computational fluid dynamics studies provide a basis for the design of the temperature control algorithm, a feedback control loop which controls the velocity of the incoming cooling air. All thermal requirements are able to be met with precise control of the ducted air and careful attention to the antenna and duct configuration.

## 2. PREDICTED PERFORMANCE

### Electromagnetic Modeling

Electromagnetic modeling was done using a combination of array factor / element factor calculations, and full-wave (moment method analysis) using Ansoft Designer. Computer memory limitations prevented us from being able to simulate the full 4x12 array using Designer. As a result, we developed two sub-aperture models for assessing the performance of the antenna in the elevation and azimuth directions. For the elevation direction, we developed a model in Designer that measured 4x4 elements. This model had a finite groundplane and allowed us to accurately characterize the antenna in its critical elevation direction. For the azimuth direction, we developed a Designer model that measured 2x12 elements. This allowed us to accurately characterize the array in the azimuth direction, particularly as a function of scan. The 2x12 array used an infinite groundplane. The basic notion underlying the use of these models is that performance along one axis is not adversely affected by elements missing along the orthogonal axis. In both cases, we endeavor to include as many elements and interconnects as possible, consistent with convergence and meshing requirements of the analysis engine.

In order to simulate the full-size array, we developed a patch element model based on the well-known cavity model, and summed the fields from an array of such elements with the appropriate coordinate transformations. This is equivalent to the array factor / element factor calculation that is commonly used in preliminary array analysis. It provides a reasonably good estimate of co-polarized performance in terms of directivity and pattern, but does not give cross-polarized performance nor input reactance.

### Gain

Antenna gain is estimated as approximately 19dBi for each polarization. The gain is estimated by first calculating the accepted gain of a 4x4 array on a finite groundplane in Designer, scaling by 4.8dB to represent a 4x12 array, and then calling this the directivity of the 4x12 array. Strictly speaking, the accepted gain as calculated by Designer includes both material losses and mismatch losses. However, our experience is that Designer tends to underestimate the material losses, and when the impedance match is good, the Designer accepted gain can be used as a conservative estimate of directivity. This value: 20.9dBi for V-pol and 20.6dBi for H-pol, are within 0.5dB of the value predicted from the array factor model. Losses due to interconnects, patch efficiency, and mismatch are estimated as approximately 1.7dB. We used the Cohn model [2] to estimate stripline losses, as modified with a correction to incorporate surface roughness [3]. The various gain constituents are summarized in Table 2.

Table 2. Gain Calculation

	V-pol	H-pol
	(dB)	(dB)
Directivity (dBi)	20.94	20.59
Total Stripline	0.710	0.660
Connector-Loss	0.120	0.120
Probe Loss	0.005	0.005
Patch Loss (85% efficiency)	0.706	0.706
Radome Loss	0.195	0.195
Total Loss	1.736	1.686
Predicted Gain (dBi)	19.20	18.90
Overall Efficiency	67%	68%

The ~19dBi net gain is the predicted gain at broadside. Gain at various scan angles is estimated by subtracting the scan loss (from full-wave analysis) from the gain at broadside.

### Antenna Patterns

The following antenna patterns are calculated from Ansoft Designer.

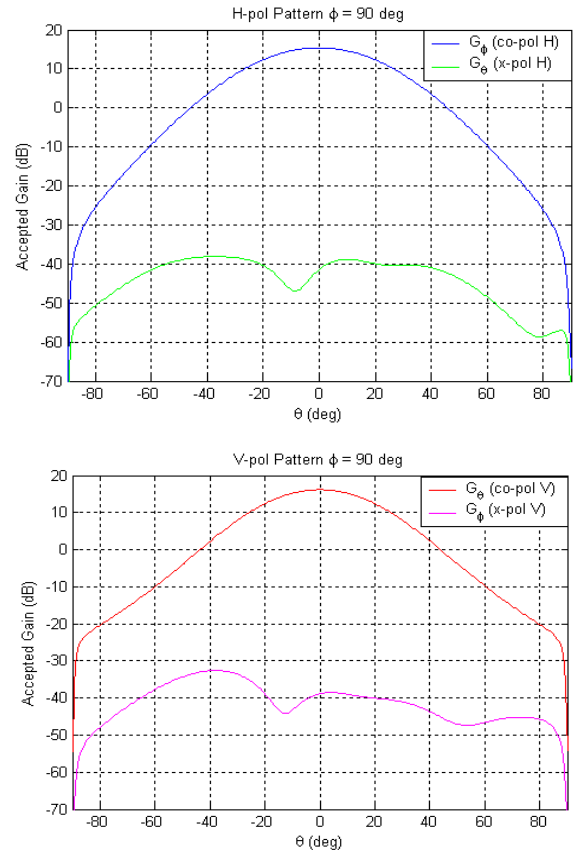


Figure 8. Predicted elevation patterns for 4x4 array

The elevation patterns have characteristic H-plane and E-plane patterns for H-pol and V-pol respectively. These patterns are similar to those generated by the array factor model, but differ subtly (particularly near end fire) because of mutual coupling in the array environment.

Table 3: Elevation performance

		H-pol	V-pol
Accepted Gain	(dBi)	20.6	20.9
3dB Beamwidth	(deg)	39.0	36.0
Sidelobe ( $\theta = -65^\circ$ )	(dB)	-27.9	-29.2
Sidelobe ( $\theta = -85^\circ$ )	(dB)	-46.6	-36.3
Pk X-pol ( $\theta < \text{HPBW}$ )	(dB)	-54	-55

The azimuth patterns are shown in Fig.9.

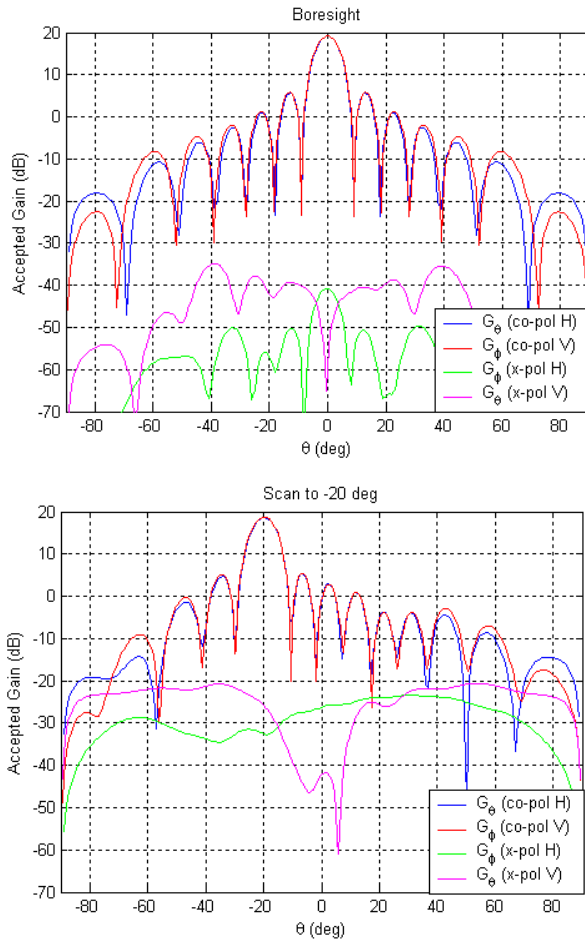


Figure 9. Predicted azimuth patterns for 2x12 array.

A summary of azimuth performance is given in Table 4. This shows the array is capable of scanning to  $\pm 40^\circ$ . However, the scan loss is 2.6dB and 1.8dB for H-pol and V-pol respectively at these scan angles, and the antenna does not meet gain and cross-pol requirements at these scan angles.

Table 4. Azimuth performance

	Scan Angle	H-pol	V-pol
Max scan angle		$\pm 40$ deg	$\pm 40$ deg
Directivity Flatness	$0^\circ$	0.45 dB	0.57 dB
Sidelobe	$0^\circ$	-13.3 dB	-13.3 dB
HPBW	$0^\circ$	8.0 deg	8.0 deg
PkX-pol ( $\theta < \text{HPBW}$ )	$0^\circ$	-60 dB	-60 dB
Directivity Flatness	$20^\circ$	0.38 dB	0.55 dB
Sidelobe	$20^\circ$	-13.2 dB	-13.3 dB
HPBW	$20^\circ$	8.4	8.4
PkX-pol ( $\theta < \text{HPBW}$ )	$20^\circ$	-47 dB	-39 dB
Scan Loss	$20^\circ$	0.57 dB	0.45 dB
Scan Loss	$40^\circ$	2.60 dB	1.81dB

Overall, the design meets sidelobe and other requirements for scan angles up to  $20^\circ$ . The cross-pol performance, as reported in Table 4, is a little misleading, as it does not reflect the cross-polarized level in the beam center on scan. This is examined more closely in the next subsection.

#### Cross-pol Performance

The cross-pol performance is estimated by first computing a series of phi-cuts every  $5^\circ$  in Designer for a 2x12 array. The co-pol and cross-pol data are then transformed according to Ludwig's 3<sup>rd</sup> definition, and are then interpolated onto a rectilinear u-v grid. The ratio of cross-pol power to co-pol power for a horizontally polarized beam scanned to  $-20^\circ$  is shown in Fig. 10. The 3dB beam contour is shown in white. The requirement is that the cross-pol ratio be less than 25dB within this contour. This is shown explicitly in the lower graphic of Fig 10, which is obtained by taking vertical slices of the pattern in u-v space that intercept the 3dB contour. A similar pattern emerges for V-pol. A small improvement in the cross-pol ratio is obtained in practice by the effective integration of the radar returns at constant elevation. Thus the antenna meets with cross-pol requirement with a comfortable margin.

#### Impedance Match

The antenna element is tuned in the infinite array environment by computing its return loss bandwidth as a function of scan angle and adjusting the element until the return loss is an acceptable value (typically better than 15dB for all frequencies of interest). We then take the element and assess its impedance match in the finite array environment for various sub-array configurations of the full 4x12 array.

It turns out that these infinite array simulations are a remarkably good predictor of impedance match performance for the finite array, even though the array configuration in our case differs markedly from the assumptions of infinite array analysis. A concurrent full-wave analysis of the interconnect board and patch element for a single antenna tile yielded an active impedance with a better than 20dB return loss. The element in the finite array was not optimized after tuning it in the infinite array,

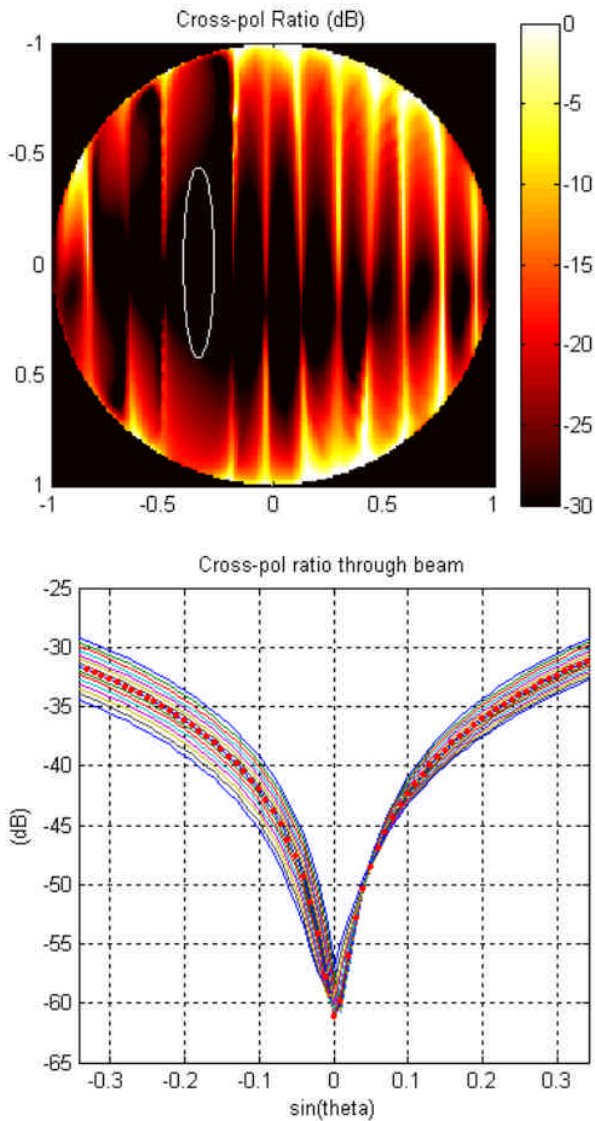


Figure 10. Cross-polarized performance for H-pol beam scanned to -20. Top: Cross-pol ratio in u-v space. Lower: Cross-section through 3dB beam contour. The dotted curve is through the center of the beam at scan angle  $u_0 = \sin(20^\circ) = 0.34$ . The beam edges in the elevation direction are  $v = \pm 0.34$  as the 3dB beamwidth is  $40^\circ$ .

Similar results are obtained for V-pol, with the difference that scan angle within 15dB return loss is about 10 degrees more for V-pol, because the scan is in the H-plane rather than the E-plane.

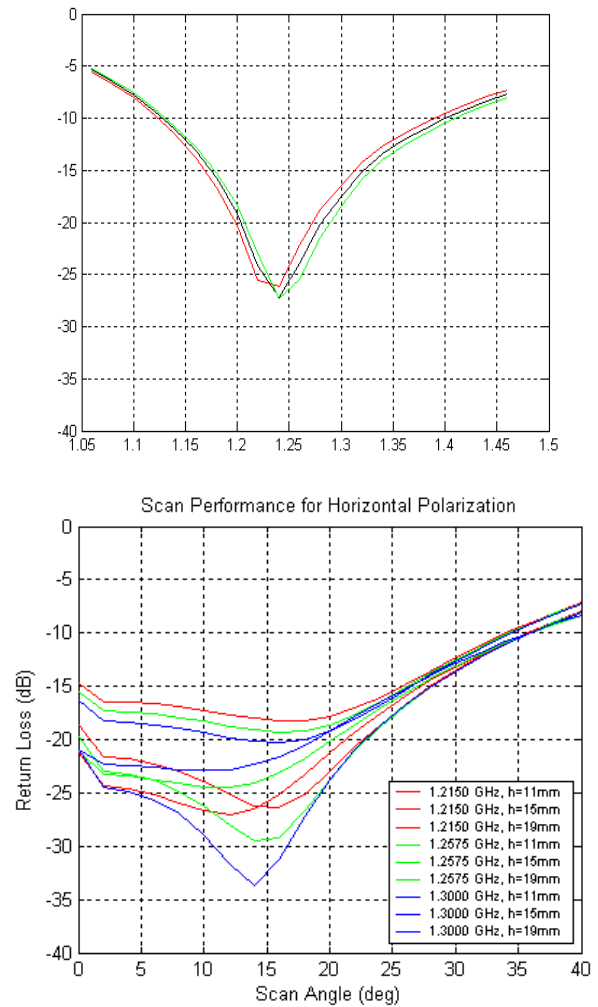


Figure 11. Infinite array reflection coefficient for h-pol. Top: As a function of frequency at broadside for different deflections of the radome. Bottom: As a function of scan angle for band center and band edges and different radome deflections.

### Phase Performance

As a key component in an interferometric instrument, phase performance of the UAVSAR antenna is critical. It is important that the phase of the antenna not vary significantly as a function of temperature, humidity, wind loading, and interaction of the antenna with the aircraft. This sub-section examines the first three of these requirements.

First, the temperature dependence of the tile was estimated using the CTEs of the tile materials. These computations also included the thermal coefficient of permittivity of the duroid substrate. It was found that path lengths varied by a small fraction of a degree and impedances varied by a small fraction of an ohm over the operating temperature range of the antenna.

Next, the impact of water, both in liquid and vapor states, was assessed. Water vapor, even at 100% relative humidity has negligible effect on antenna performance at L-band. Water in liquid form has a more noticeable impact. Water vapor in the honeycomb cells of the radome, antenna tile, or the intervening space between tile and radome can potentially condense and form a thin dielectric film “coating the antenna”. Worst case analysis shows this film to be approximately 0.1mil in depth, causing the far-field phase of the antenna to vary as much as 2°. It is anticipated that water, condensed or otherwise, will be purged from the antenna between flights, thus avoiding the problem of cumulative deposits of water.

Last, the impact of wind loading was assessed by running infinite array and isolated element simulations with radome heights varying over the anticipated deflection range. The analysis shows that a radome height of 15mm will result in a phase variation of less than 0.1 degree per millimeter, which corresponds to less than ±0.5 degree for a ±4mm deflection.

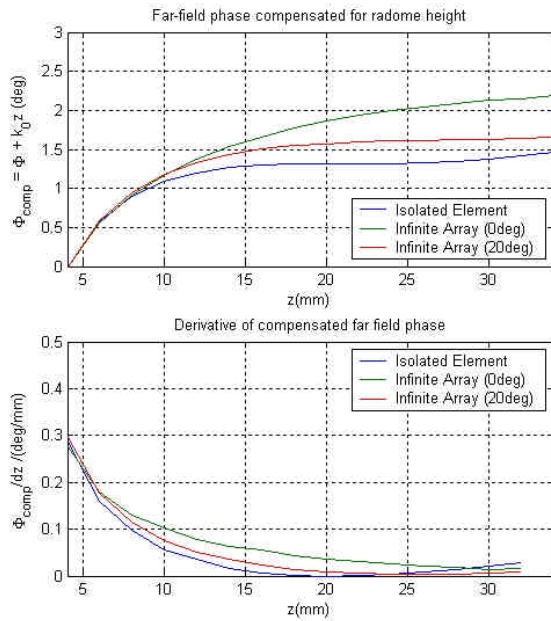


Figure 12. Phase variation as a function of radome height. The phase response is compensated to account for the fact that the far field phase is computed relative to the top of the radome. The lower graph shows the far-field phase derivative with respect to radome height.

### Accommodation Analysis

A significant amount of effort was put into designing an antenna that has an acceptably low level of interaction with the aircraft. Fig. 13 shows the antenna pod located below a Gulf Stream aircraft platform. The along-flight center of the antenna is located 0.8m behind the leading edge of the wing (at the point where it joins the fuselage). The elevational center of the antenna is 0.87m below the wing. Hence the antenna is mostly ahead of the wing, but there potential for scattering, particularly as the beam is scanned back towards the wing. This is evident from the geometry of the antenna and aircraft wing. The plane of the antenna is oriented at an angle of 45° from vertical. Energy at grazing incidence (-90°) has the potential to reflect and/or diffract from the wing and interfere with the pattern of the main beam. Other scattering mechanisms are possible, but are less likely to be as problematic.

Using the antenna pattern of an untapered 4x12 antenna array, we found that this multipath interference was unacceptably high. Consequently, we derived a requirement that the antenna pattern near grazing incidence must be 30dB below the peak gain between 85° and 90° in order to produce acceptable phase and amplitude ripple in the main beam.

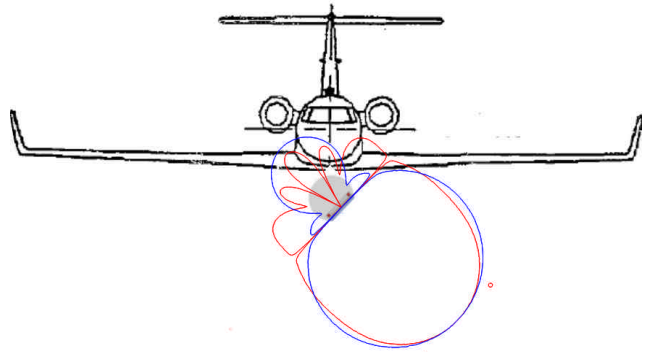


Figure 13. Gulf Stream and radar pod configuration. The overlaid antenna patterns are H-pol (blue) and V-pol (red)

The basis for this analysis was a PO/PTD program called GRASP that uses a tabulated feed derived from an array factor model. An array factor model was chosen as the input to the PO/PTD analysis for two reasons. First, it is possible to generate the co-polarized pattern reasonably accurately over all space for the complete array. Second, our full-wave analysis code, Designer, generates artificial nulls in the pattern at 90 degrees – the very place where we want to accurately model the pattern.

To this end, we modified the element factor code so that the element pattern near 90 degrees in the elevation direction ( $\phi=90^\circ$ ) more closely resembled the patterns seen in full-wave analysis. These data were imported into the GRASP program and were used to synthesize a spherical wave expansion. This allows the PO/PTD engine to accurately calculate the reflected and diffracted fields from the wing structure, which are in the near field of the antenna. The PO/PTD data for the antenna with and without wing are then compared by subtraction; the result being an error pattern that represent the effect of multipath.

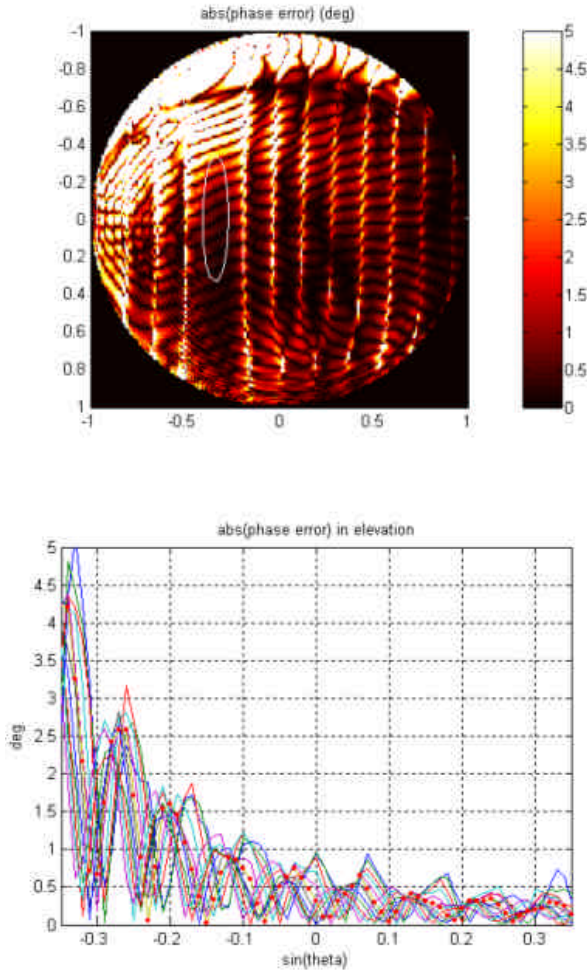


Figure 14. Phase error due to multipath scattering from aircraft wing. V-pol beam scanned  $-20^\circ$ . Top: Absolute phase error over u-v space. Bottom: absolute phase error through 3dB beam.

Fig. 14 shows that the phase ripple for vertical polarization is less than 2.5 degrees over most of the 3dB beam, except at the very edge of the far-range beam, where the ripple becomes approximately 4.5 degrees. The corresponding amplitude ripple is less than 0.4dB over most of the 3dB beam. Similar results emerge for horizontal polarization. These levels of interference have been deemed acceptable by subsequent systems analysis.

### 3. CONCLUSIONS

This paper has presented the design of phased array antenna aperture that meets demanding performance, environmental, and accommodation requirements for application in UAV-based radar interferometry. The current status of the development at time of writing is that an antenna tile breadboard is currently undergoing antenna range measurements for patterns and gain. Subsequently, the antenna tile will undergo high-power ionization breakdown testing at simulated altitude at the JPL Bell Jar facility. It then will be subjected to thermal cycling and shake testing. At JPL. The results of these measurements and tests will be reported at the conference.

The research described in this paper was carried out at the Jet Propulsion Laboratory, California Institute of Technology, under a contract with the National Aeronautics and Space Administration.

### 4. REFERENCES

- [1] N. F. Chamberlain, et al., "Microstrip Patch Antenna Panel for Large-Aperture L-band Phased Array," Proc. 2005 IEEE Aerospace Conference, Big Sky, MT, 2005.
- [2] S. B. Cohn, "Problems in strip transmission lines," IRE Trans. Microwave Theory Tech., vol.MTT-2 pp.119-126, Mar. 1955.
- [3] S. Sundstrom, "Stripline Simulation Models with Conductor Roughness", Master's Thesis, Helsinki University of Technology, 2004.

### 5. BIOGRAPHIES

*Neil Chamberlain* received the B.Sc. degree with Honours in Electrical Engineering from King's College London, UK in 1981. He worked briefly for Marconi Space and Defense Systems, Ltd., Portsmouth, UK before undertaking graduate studies at The Ohio State University, where he received the M.S. and Ph.D. degrees in Electrical Engineering in 1984 and 1989. He was a professor at the South Dakota School of Mines and Technology in Rapid City, South Dakota between 1990 and 2003. His research focused on ultra-wideband phased array radar antennas and systems. He is currently a Senior Engineer with JPL's Spacecraft Antennas Group, where he is working on large aperture antennas and active phased arrays. Dr. Chamberlain is a member of Eta Kappa Nu and Tau Beta Pi.

*Gregory Sadowy* received the B.S. in Electrical Engineering from the Rensselaer Polytechnic Institute in 1992 and the

*Ph.D from University of Massachusetts at Amherst in 1999, where he specialized in development of radar systems for Earth remote sensing. Dr. Sadowy is currently a Senior Engineer in the Radar Science and Engineering Section at the Jet Propulsion Laboratory where he has worked on development of millimeter-wave radar systems for cloud and rain measurements and radar technology, antennas and systems for Earth and planetary remote sensing and landing in the frequency range of 1-180 GHz. He is currently Cognizant Engineer for the UAVSAR Active Array Antenna and Principal Investigator for a task developing active array technology for 160 GHz landing radars..*

***Eric Oakes** received a B.S. in Metallurgical Engineering from The University of Washington in 1999. He is currently working at the Jet Propulsion Laboratory in the Materials and Processes Group focusing on the design and fabrication of composite spacecraft parts. While at JPL he has been involved in the design and fabrication of composites for several space projects including Mars Pathfinder, Mars Exploration Rover (MER), Deep Impact, and GALEX.*

***Kyle Brown** received the B.S. degree Summa Cum Laude from The Ohio State University in Mechanical Engineering in 2003. In 2004, he received the M.S. in Mechanical Engineering from Ohio State where his research focused on adaptive control theory and mechanism design. He is currently in the Instrument Structures and Configuration group at the Jet Propulsion Laboratory. Kyle was a recipient of the Mars Exploration Directorate Team Award for his work on the 2007 Phoenix Mars Lander.*

***Richard Hodges** received the B.S.E.E. degree from University of Texas at Austin, the M.S.E.E. degree from California State University, Northridge, and the Ph.D. in Electrical Engineering at University of California, Los Angeles. From 1978-1984 he was with the Hughes Aircraft Company Radar Systems Group. In 1984 he joined the Adams-Russell Microwave Products Division in Chatsworth, CA (now Rantec). In 1988 he joined NASA's Jet Propulsion Laboratory where he developed reflector antenna analysis software for the Deep Space Network. In 1997 he joined Raytheon's Antenna/Nonmetallics Technology Center in McKinney, Texas where he led development of the world's first decade bandwidth phased array antenna. Since 2001 he has been with JPL, where he currently heads the flight Spacecraft Antennas Group. At JPL, he has led development of a reflectarray for ocean surface height altimeter and has contributed to development of active array technology for space based radar..*